J. Earth Syst. Sci. (2020)129 59
https://doi.org/10.1007/s12040-019-1324-1

A new Western Disturbance Index for the Indian winter monsoon

T M Midhuna, P Kumar and A P Dimri*

School of Environmental Sciences, Jawaharlal Nehru University, New Delhi, India.
**Corresponding author. e-mail: apdimri@hotmail.com*

MS received 28 May 2019; revised 9 October 2019; accepted 26 October 2019

The Himalayas are storehouse of freshwater, which is of utmost importance for agriculture and power generation for billions of people in India. Winter (December, January and February: DJF) precipitation associated with Western Disturbances (WDs) influences Himalayan climate, glaciers, snow-water storage, etc. One-third of annual precipitation over northern Indian region is received during winter. Winter WDs are synoptic-scale systems embedded the subtropical westerly jet (SWJ). Their orographic interaction with the Himalayas intensifies precipitation over Pakistan and northern India. Precipitation due to WDs and associated dynamics are termed as Indian winter monsoon (IWM). The present study focuses on the WDs climatology using National Center for Environmental Prediction/National Center for Atmospheric Research, US (NCEP/NCAR) reanalysis data. The period of study spans over 29 years (1986–2016) during which ∼500 WDs were observed as per India Meteorological Department (IMD) daily weather report. Precipitation, vertical distribution of wind and geopotential height during the passage of these WDs are analyzed. Importantly, a new index, Western Disturbance Index (WDI), for measuring strength of IWM is proposed by using difference of geopotential height at 200 and 850 hPa levels. The index is able to capture changes in 500 hPa wind, air temperature and mean sea level pressure during the passage of WDs.

Keywords. Western Disturbance Index (WDI); Indian winter monsoon (IWM); western disturbances (WDs); subtropical westerly jet (SWJ).

1. Introduction

Indian winter monsoon (IWM) is defined as winter precipitation due to western disturbances (WDs), embedded in large scale subtropical westerly jet (SWJ) and associated circulation dynamics during winter (Dimri *et al.* 2016). During winter, northwest India receives 1/3rd of its annual precipitation. This precipitation is important for the production of Rabi crops and to maintain glaciers. Winter precipitation provides moisture and low temperature for the development of these winter crops and is therefore important for an agrarian dependent economy of the country (Benn and Owen 1998). IWM is important for glaciers and its spring/summer snowmelt contributes water for agriculture, power generation as well as socio-economic needs (Rees and Collins 2006; Immerzeel *et al.* 2010). IWM (Dimri 2013a, b; Dimri and Niyogi 2013; Yadav *et al.* 2013) studies are less compared to Indian Summer Monsoon (ISM) (Krishnamurti and Bhalme 1976; Webster 1983; Goswami 1994). Most of the climate research community is focussed on ISM because it is the

Supplementary materials pertaining to this article are available on the Journal of Earth Science Website (http://www.ias.ac.in/Journals/Journal_of_Earth_System_Science).

Published online: 22 January 2020

lifeline for millions of people in the Indian subcontinent and contributes 70% of annual rainfall over Indian region (Ashok *et al.* 2004). IWM is limited over northern Indian region, but is important in respect to Himalayan climate and hydrology (Dimri 2013b). The intensity of IWM decreases with east and southward progression (Yadav *et al.* 2012). Due to its contribution to mass balance of glaciers, IWM studies are important in the context of global warming (Bookhagen and Burbank 2010). Seasonal snowfall and its frequency show a decreasing trend in winter (Shekhar *et al.* 2010). But some studies show increase in winter precipitation over northwestern part of India during recent period (Dash *et al.* 2007; Yadav *et al.* 2010).

Winter precipitation is mainly due to the eastward-moving synoptic weather system known as WDs (Pisharoty and Desai 1956; Rao and Srinivasan 1969; Mooley 1957; Dutta and Gupta 1967; Mohanty *et al.* 1998). It originates from Mediterranean/Caspian Sea with frontal characteristics similar to that of extratropical storms (Dhar *et al.* 1984) but gradually loses its frontal nature due to lowering of pressure and temperature gradients (Rao and Rao 1971). Moreover, it gets intensified due to incursion of moisture from Caspian and Arabian Seas and interaction with Himalayan topography which results in increased precipitation (Singh *et al.* 1981; Dimri and Niyogi 2013). Hunt *et al.* (2018a) assessed moisture sources for drought, median and heavy rainfall events during winter season using Lagrangian method. Their study revealed that sources of moisture are different during each event. The source of moisture during dry events was from Arabian peninsula. For median rainfall event, the air parcels originated in the Arabian peninsular region and Oman. For the wet case, air parcels having originated from Persian Gulf were associated with cyclonic disturbances over the Hindustan domain which advects northerlies and is found to co-occur with passing WDs observed by Hunt *et al.* (2018b). Thermo-dynamical study of WDs highlight that additional source of moisture is required for the precipitation related to WDs. Convective activity is detected as the increase in value of convective available potential energy (CAPE) during the propagation of WDs (Roy and Bhowmik 2005).

The amount of precipitation received in the Himalayas is not linearly linked with the dynamics associated with the intensity of WDs (Lang and Barros 2004). WDs propagate over different countries such as Iran, Iraq, Afghanistan, Pakistan and India and affect the weather over these regions and become intense during winter. About 50% of annual precipitation over Karakoram Himalaya is obtained due to the passage of WDs in winter (Barros *et al.* 2006). Associated extreme precipitating events during winter are harmful to nature (Dimri and Chevuturi 2014). WDs do not always have well-marked cold or warm fronts either at the surface or upper levels. This is how WDs differ from extratropical depressions (Mooley 1957). WDs are embedded in subtropical westerly jet (STJ) which provides upper-level divergence for the intensification of WDs (Puranik and Karekar 2009). WDs are analyzed through its vertical structure (Hunt *et al.* 2018b). Their analysis of vertical distribution of zonal wind of tracked WDs indicates westerly jet which is strongest at 200 hPa. Mean jet speed of 40 m/s is noted ahead of WD. A strong cyclonic circulation with wind speed of 10 m/s is observed at upper troposphere in the vertical cross-section of meridional wind. WDs have a lifecycle of 3–4 days (Dutta and Gupta 1967). But it may differ in accordance with the intensity of WDs. If multiple WDs occur continuously it may have a longer life span. WDs move eastwards at a rate of 5° longitudes per day. Winter months record 6–7 WDs per month but its frequency decreases in summer (Rao and Srinivasan 1969). Mohanty *et al.* (1998) reported the occurrence of 4–6 WDs during the winter season (November–March). The occurrence of WDs over a region does not ensure precipitation as it depends on the availability of moisture and instability conditions during its propagation. WDs form a trough in westerlies at 500 hPa level. The position of trough in westerlies determines the strength and vertical extent of it.

Geopotential height is commonly used by the scientific community to study WDs because deep trough within the extratropical cyclones exhibits distinctive signature. Heavy precipitation events over central Himalaya (CH) are associated with 500 hPa geopotential height and this relation is used by Lang and Barros (2004) to analyze WD activity. An increase in precipitation is linked with more troughs in westerlies which is related to increased variability in 500 hPa height. Cannon *et al.* (2015) studied frequency and magnitude of WDs using 200 hPa geopotential height anomalies and found enhancement in WDs activity leads to local heavy precipitation over Karakoram/western

Himalaya (KH) and CH. Ridley *et al.* (2013) predicted future WDs activity using projections from a regional climate model. An increase in the occurrence of WDs and snowfall is observed by 2100. An increase in heavy precipitation events over western Himalaya (WH) in recent decades is linked to increased baroclinicity of the westerly winds which enhanced variability of WDs (Madhura *et al.* 2015). They constructed a quantitative index describing the activity of WDs using 500 hPa geopotential height.

Sometimes, these WDs in association with other local/synoptic-scale weather systems cause severe weather such as hailstorms leading to destruction of property and crops (De *et al.* 2005); avalanches which result in collapse of snow cover in the mountains (Rangachary and Bandyopadhyay 1987); fog under stable atmospheric conditions, i.e., moisture availability along with low wind speed (Rao and Srinivasan 1969; Syed *et al.* 2012), and cold waves associated with the departure of temperature from normal minimum temperature (Mooley 1957). Thus in recent times with concurrent understanding, it becomes imperative to understand WDs.

The present study focuses on investigating the percentage contribution of winter precipitation due to WDs and proposes a Western Disturbance Index (WDI) using the difference of 850 and 200 hPa geopotential height. Characteristics of WDs are analyzed using this index to correspond it with the possibility of future prediction and associated dynamics.

2. Data and methods

2.1 *Data*

Precipitation data used in this study are obtained from the Climate Prediction Centre (CPC) global daily unified gauge-based analysis of precipitation (Chen *et al.* 2008). The data is available at 0.5° resolution over global land areas, starting from 1979. The data comprises historical observations, satellites, radars and numerical model forecasts to maintain higher precision. Orographic effects are also considered in creating precipitation data (Xie *et al.* 2007). National Center for Environmental Prediction/National Center for Atmospheric Research (NCEP/NCAR) (Kalnay *et al.* 1996) daily mean reanalysis of surface air temperature, wind and geopotential height at different levels, omega at 500 hPa, and mean sea level pressure (MSLP) for the winter period 1986/1987 to 2015/2016 is also used. The resolution of the NCEP/NCAR reanalysis is at 2.5° with 12 pressure levels from 1000 to 100 hPa. The WD index is developed using NCEP/NCAR data. In order to validate the index, Era-Interim reanalysis data with spatial resolution of 0.75° provided by European Centre for Medium-Range Weather Forecasts (ECMWF) (Dee *et al.* 2011) is used. The number of WDs for the study period is obtained from Indian Daily Weather Reports (IDWR) of the India Meteorological Department (IMD) which provides daily observations recorded at 0830 hrs IST. The WDs number per season for each year are provided in table 1.

2.2 *Methods*

More than 500 cases of WDs are analyzed during the study period. Changes in pressure, temperature and

Table 1. *Number of WDs occurred during winter season (December, January, February – DJF) per year during 1986–2016 period*

Year	No. of WDs
1987	23
1988	21
1989	24
1990	18
1991	20
1992	19
1993	19
1994	17
1995	26
1996	25
1997	20
1998	19
1999	18
2000	14
2001	16
2002	20
2003	21
2004	26
2005	21
2006	21
2007	21
2008	23
2009	19
2010	23
2011	17
2012	14
2013	18
2014	16
2015	10
2016	13

wind occur during the passage of WDs both at the lower and upper troposphere (Dimri 2006). For this reason, we have used lower (850 hPa) and upper (200 hPa) tropospheric geopotential height for constructing WDI. The thickness between 850 and 200 hPa level is proportional to mean temperature as well as moisture of air between those levels. Empirical Orthogonal Function (EOF) method is used for analyzing variability of geopotential height, zonal wind and meridional wind. The spatial pattern of variability and its time variation is identified from this method. Spatial patterns are known as EOFs and time series are known as Principal Components (PCs) (Wilks 1995; Kutzbach 1967; Jolliffe 2002). The first pattern explains largest part of the variance and second pattern explains largest part of the remaining variance and so on.

3. Results and discussion

The topography of the study area is shown in figure 1. Most WDs are found to be concentrated within the large box of area 25–40°N, 60°–80°E and is therefore considered for the present study. A smaller box of area 32–37°N, 70–77°E is used to average precipitation in the present study. WH receives considerable amount of precipitation during winter as WDs interact with Himalayas thus providing orographic forcings. The following sections elaborate on the basic fields, and thereafter on WDI.

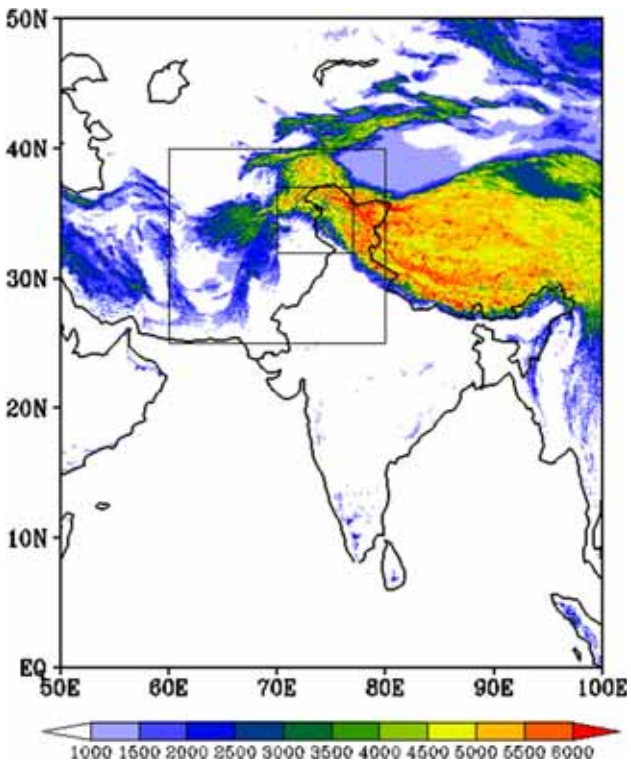

Figure 1. Topography (m: shade). The area of 25–40°N, 60–80°E is considered to define the Western Disturbance Index (WDI). The area of 32–37°N, 70–77°E is considered for averaging precipitation in the present study.

3.1 *Basic fields*

Precipitation climatology of WDs and non-WD days during winter is shown in figure 2. A higher amount of precipitation is obtained during WD days over Karakoram, Hindukush and Sulaiman ranges (figure 2b). Heavy precipitation occurs near hilly areas due to the complex orographic interaction of WDs with high mountain ranges (Dimri and Niyogi 2013). Though not all the WDs precipitate heavily, few of them produce heavy precipitation. WDs cause heavy precipitation in WH usually in the form of snow (Ridley *et al.* 2013). Winter precipitation is the sum of WD days and non-WD days precipitation (figure 2a). Non-WD days produce lower amount of precipitation (figure 2c). The average amount of precipitation during DJF is less than that of WD days. To analyze spatial variability, average precipitation during DJF is subtracted from the mean precipitation during WDs (figure 2d). Higher precipitation during WD days than DJF is observed over Karakoram region. Similarly, average precipitation during non WDs is subtracted from WDs in figure 2(e). Higher precipitation over WH, Hindukush and Sulaiman ranges indicates that large amount of precipitation is obtained over this region during WD days compared to non-WDs.

Percentage precipitation for WDs and non-WD days is shown in figure 3(a and b) respectively. WDs contribute 80% of winter precipitation over Afghanistan, Pakistan and northern India. This winter precipitation is mainly due to the interaction of WDs with the Himalayas. In non-WD days, ∼20% of winter precipitation over Afghanistan, Pakistan and northern India is observed. WH is characterized by heterogeneous topography with highly nonlinear land–atmosphere interactions. Interaction of WDs with WH determines amount of winter precipitation obtained over the region. Precipitation is mostly in the form of snow over WH (Dimri 2012). The water budget over the high mountain areas depends on the topography and land use of the area (Fairman *et al.* 2011).

The spatial distribution of seasonal precipitation cannot completely distinguish the behaviour of precipitation during DJF and WD days. Therefore,

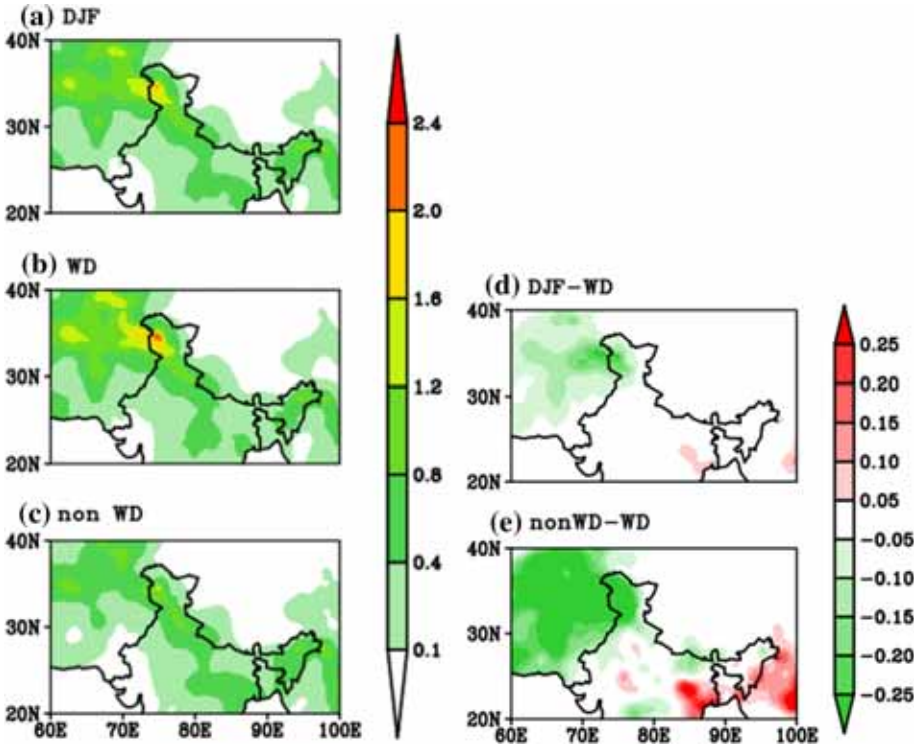

Figure 2. Precipitation climatology (mm/day) in (**a**) December, January, February (DJF) (**b**) WD days of DJF (**c**) non-WD days of DJF (**d**) DJF-WD days (**e**) nonWD-WD days averaged during 1986–2016 period. In figure (**d**) and (**e**) negative values indicate higher precipitation during WD days compared to DJF and non-WD days.

the frequency distribution of precipitation is plotted during DJF and WD days to better understand the spatial variability of precipitation intensity. The entire range and frequency of precipitation can be estimated in a more coherent manner by this method. DJF and WD days mean precipitation intensity along with their frequency in percentage is plotted (figure 4). The probability distribution function is plotted as gamma distribution curve. Gamma distribution is an excellent choice for describing precipitation parameters in areas with low mean and high variability in precipitation (Husak *et al.* 2007). The extended tail to the right of the distribution is advantageous in representing extreme rainfall events (Ananthakrishnan and Soman 1989). Flexibility in shape of the gamma distribution function allows it to fit any number of rainfall regimes. Each curve is identified with two parameters: shape parameter (α) and scale parameter (β). There is a close resemblance in shape parameter, α between DJF and WD curve. Most of the precipitation is concentrated in the range of 0.6–0.8 mm/day for both DJF and WD. But the frequency of peak precipitation in the intermediate range is slightly higher for DJF. Longer tail observed in the WD curve indicates that high precipitation ranges are seen during WD days.

In order to verify the major amount of precipitation during WD days due to the occurrence of WDs, the correlation map between monthly precipitation and monthly WD days is plotted and is shown in figure 5. Correlation coefficients of 0.4–0.6 are seen over the northwest part of India and associated regions during the month of December. The low correlation coefficients are due to non-homogenous in situ station data obtained in these high altitude regions. The complex orography of the region is an obstacle to monitoring precipitation. Most of the in-situ stations are situated in low altitude regions, and very few are present in mountain tops where there is a chance for heavy precipitation (Archer and Fowler 2004). Thus precipitation in high altitude regions is not measured. Snowfall in high altitude region is also poorly measured (Rasmussen *et al.* 2012).

Figure 6 shows an interannual variation of precipitation during DJF, WD days of DJF and non-WD days of DJF during 1986–2016 period. Precipitation is area averaged over the region 32°–37°N, 70°–77°E. Cumulative averaged precipitation is more during WD days compared to

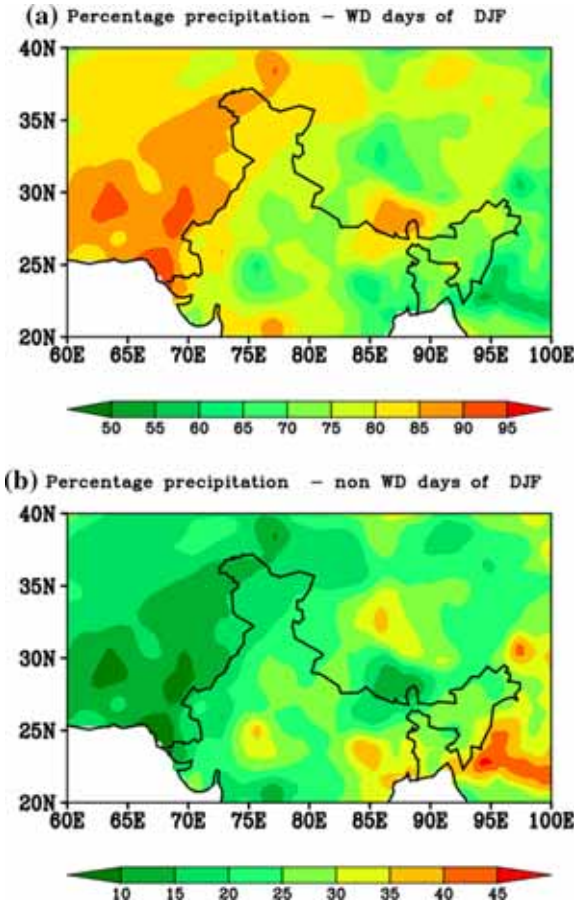

Figure 3. Percentage precipitation in (**a**) WD days of DJF and (**b**) non-WD days of DJF averaged during the 1986–2016 period. WD days contribute 80–90% of precipitation over western Himalayas.

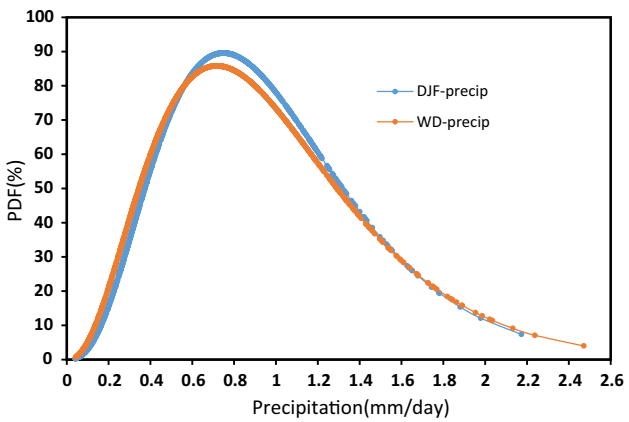

Figure 4. Probability Distribution Function (PDF) for rainfall intensities during DJF and WD days of DJF over 1986–2016 period.

non-WD days. WD days and DJF show almost similar precipitation amount except during few years. As shown in figure, in years 1987, 2006, and 2014 higher precipitation during non-WD days is received as compared to other years. Higher

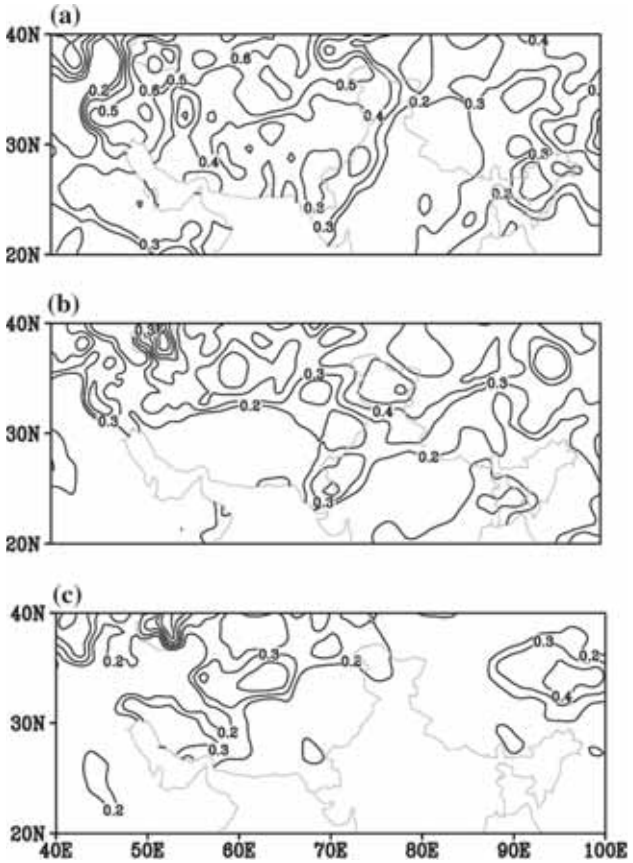

Figure 5. Correlation between monthly precipitation and monthly WD days for (**a**) Dec, (**b**) Jan and (**c**) Feb during the 1986–2016 period. Shown in contours are correlation coefficients.

precipitation is observed during DJF and WD days in 2009 and 2013. About 19 and 18 WDs occurred in these years, respectively. In the year 2013, non-WD days show nil precipitation. So, precipitation during 2013 winter is mainly due to WDs. In addition, in year 2014, non-WD days yield higher amount of precipitation. These anomalous cases need further investigation and study in future.

Longitudinal versus vertical cross-sectional distribution of zonal wind, meridional wind and geopotential height and specific humidity averaged over 20–40°N latitude is shown in figure 7a–d. The maximum zonal wind is observed at mid- to upper-troposphere over 60–80°E longitude with core of maxima at 300 hPa. The higher meridional wind is found over 70–85°E from 700–100 hPa. Negative values of geopotential height are also observed from mid- to upper-troposphere. Further, latitudinal versus vertical cross-section of these variables averaged over 60–100°E longitude is shown in figure 7e–h, respectively. Zonal wind maxima are found at 250 hPa over 20–35°N latitude,

meridional wind maxima at 300 hPa over 30–40°N latitude and negative geopotential height minima at 300 hPa over 25–40°N latitude. Positive (negative) values of zonal wind denote westerly (easterly) wind (wind coming from west (east)). Similarly, positive (negative) value of meridional wind indicates southerly (northerly). Negative values of geopotential height indicate low-pressure area or trough which mainly occurs during precipitating WDs (Dimri 2006). A maximum geopotential anomaly is found at 200 hPa. Comparatively fewer values are found at 500 hPa level. But 500 hPa geopotential height is the commonly used variable to represent atmospheric circulation and is also used to predict other meteorological variables (Zheng and Frederiksen 2007). A trough is associated with cloudy conditions and precipitation or it can bring in cold air mass. These figures indicate that southwesterly wind and trough forms over northwest part of India during the passage of WDs. The southwesterly wind brings moisture from Arabian Sea which leads to widespread precipitation over WH. Seasonal anticyclone formed over central India at 0.9 km above sea level controls this moisture intake (Rangachary and Bandyopadhyay 1987).

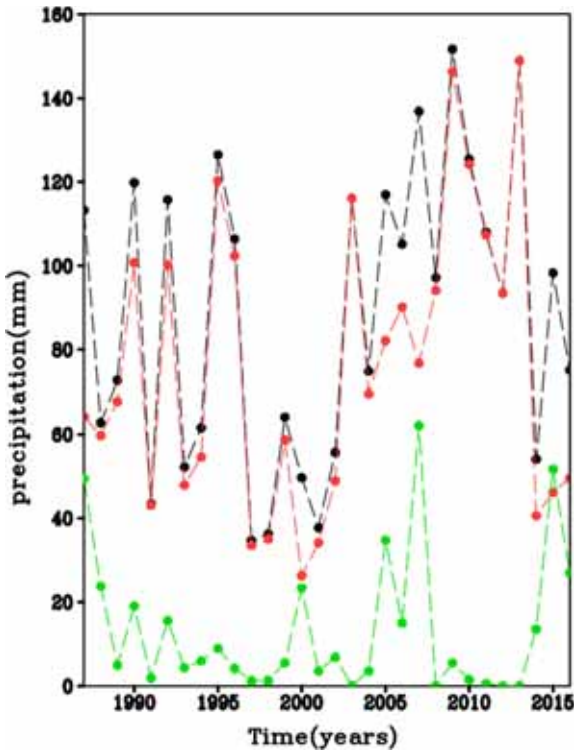

Figure 6. Time-series of cumulative seasonal precipitation (mm) during DJF (black line), WD days of DJF (red line), non-WD days of DJF (green line) averaged over the region (32–37°N,70–77°E) during 1986–2016 period.

Specific humidity is used to describe the moisture field in the present study. It is the ratio of the mass of water vapour to total mass of air. Wet anomaly is found in the lower troposphere. As we go upwards moisture content decreases and dry

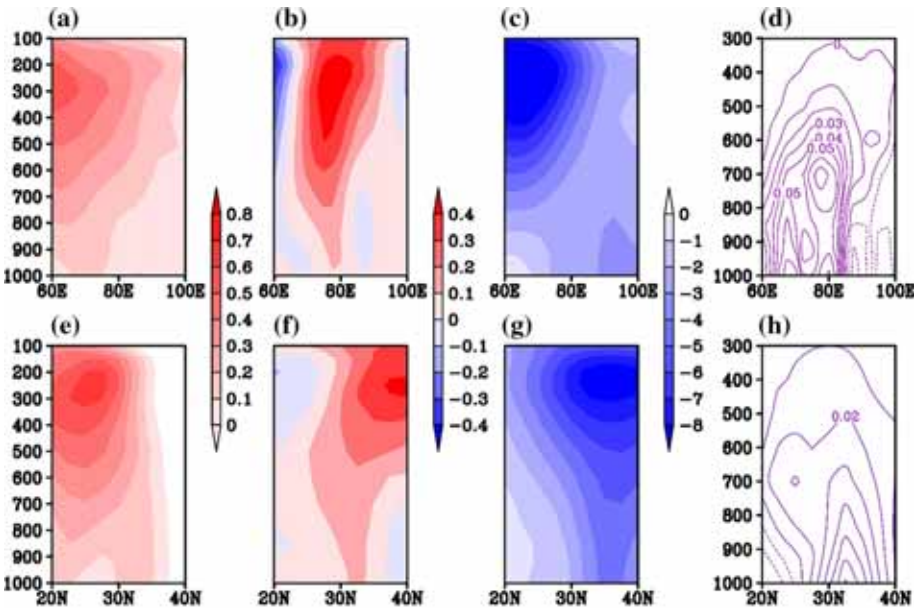

Figure 7. Longitude-pressure vertical cross-section averaged over 20°–40°N latitude for (**a**) Zonal wind(m/s) (**b**) Meridional wind (m/s) (**c**) Geopotential height (m) (**d**) Specific humidity (g/kg). Latitude-pressure vertical cross-section averaged over 60°–100°E longitude for (**e**) Zonal (m/s) (**f**) Meridional (m/s) and (**g**) Geopotential height (m) (**h**) Specific humidity (g/kg) of (WD minus DJF) days during 1986–2016 period. Positive zonal and Meridional wind denotes south westerly wind and negative Geopotential height indicates low-pressure area or trough.

anomaly is seen in the mid-upper troposphere (figure 7d). Changes in specific humidity are more observed in the longitude–pressure vertical cross-section.

Omega at 500 hPa is used to analyze vertical motion (ascending or descending motion) of air/mass and is shown in figure 8. Negative values of omega indicate ascending motion of air and positive values imply descending of air. The upward motion of air leads to increase in relative humidity through large depth of atmosphere which further results in clouds and precipitation. On the availability of moisture in vertical air column due to incursion from Arabian Sea, possibility of precipitation forming mechanism will be expedited. Negative values of omega i.e. strong ascend is seen ahead of WDs over WH during the passage of WDs which is found to be maximum at 450 hPa followed by a descending (Hunt *et al.* 2018b) which leads to strong upward movement of air, as a result orographic lifting of moisture occurs.

Circulation and geopotential height at 200, 500 and 850 hPa are illustrated in figure 9(a–c) respectively. Geopotential height is plotted in contours. A strong band of negative geopotential is seen between 25 and 50°N latitude centered at 200 hPa (figure 9a) along with southwesterly winds traveling from western part of continent towards northwest part of India and WH region. The strong westerlies are capable of bringing moisture from Arabian Sea which thus will sustain WDs and leading to intensification of IWM. A similar distribution of westerlies is seen at mid-tropospheric levels with lesser magnitude (figure 9b). At lower troposphere westerlies are not seen (figure 9c). The upper-level cyclonic situation which developed due to strong westerlies is able to ascend the moisture rapidly resulting in cloud formation and heavy precipitation over the region.

The difference between geopotential height anomalies at 850 and 200 hPa is calculated over the region 25–40°N, 60–80°E and is shown in figure 11(a). This region is selected as maximum dynamics associated with WDs and associated precipitation occurs over here. Dimri and Chevuturi (2014) established that vertical distribution of geopotential height anomaly shows a northwestern tilt in vertical axis of the WDs. During early stage of WDs, the low-pressure region shows northwestern tilt which becomes northeasterly with subsequent propagation of WDs. Thus vertical difference between 850 and 200 hPa is proportional to volume over the specified region which further depends on mean temperature of air between these levels. The thickness of air is a measure of coldness or warmness of air. Geopotential height anomaly at upper level is low during winter compared to lower level. Geopotential height anomaly at upper troposphere is subtracted from lower troposphere results in large positive value during winter season. As shown in figure 11(a) values start increasing from November onwards and attain maximum value in January and February and after that it starts decreases.

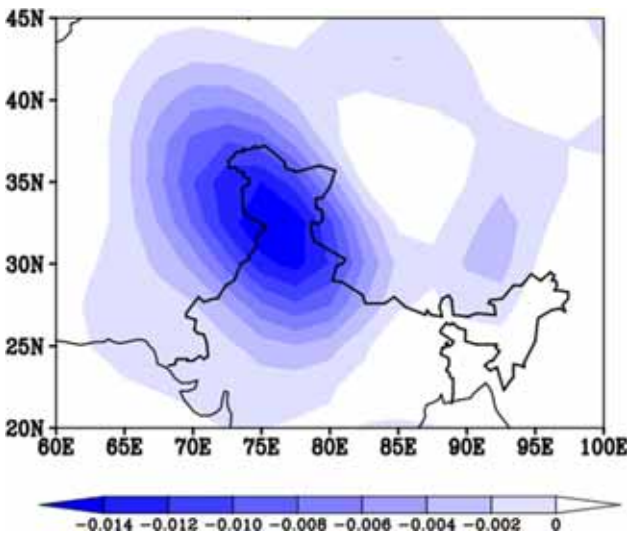

Figure 8. Omega (Pa/s*10^{-3}) at 500 hPa of WD averaged during the 1986–2016 period. Negative omega values show upward motion.

3.2 *Western Disturbance Index*

Winter WDs have asymmetric upper air trough which has similar characteristics of Bjerknes cyclones of pacific and Atlantic (Pisharoty and Desai 1956). The energy discharge and development of WDs can be explained by baroclinic instability (Rao and Rao 1971). This instability arises due to the meridional temperature gradient. WDs which result in heavy precipitation, has deep upper-level trough which is located westward and shows vertical tilting (Cannon *et al.* 2015). Model analysis indicates a northwestern tilt in geopotential anomaly during the early growth stage of WDs (Dimri and Chevuturi 2014). Cyclones growing by baroclinic processes are expected to tilt upshear. This westward tilt is important because potential energy is provided to the disturbance by mean flow through this (Holton and Hakim 2012). The

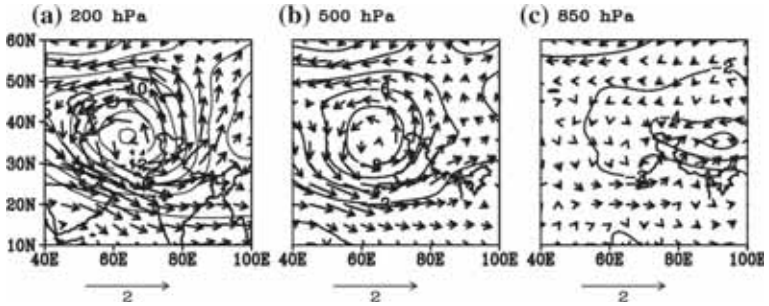

figure 9. Wind (m/s: vector) and geopotential height (m: contour) for (WD minus DJF) days at (**a**) 200 hPa, (**b**)500 hPa and (**c**) 850 hPa averaged during 1986–2016 period. Stronger south westerlies and trough occurs at middle and upper troposphere.

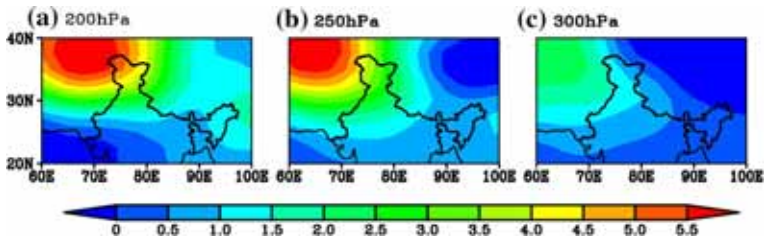

Figure 10. Potential vorticity (10^{-8} K kg^{-1} m^{2}s^{-1}) for (WD minus DJF) days at (**a**) 200 hPa, (**b**) 250 hPa (**c**) 300 hPa averaged during 1986–2016 period.

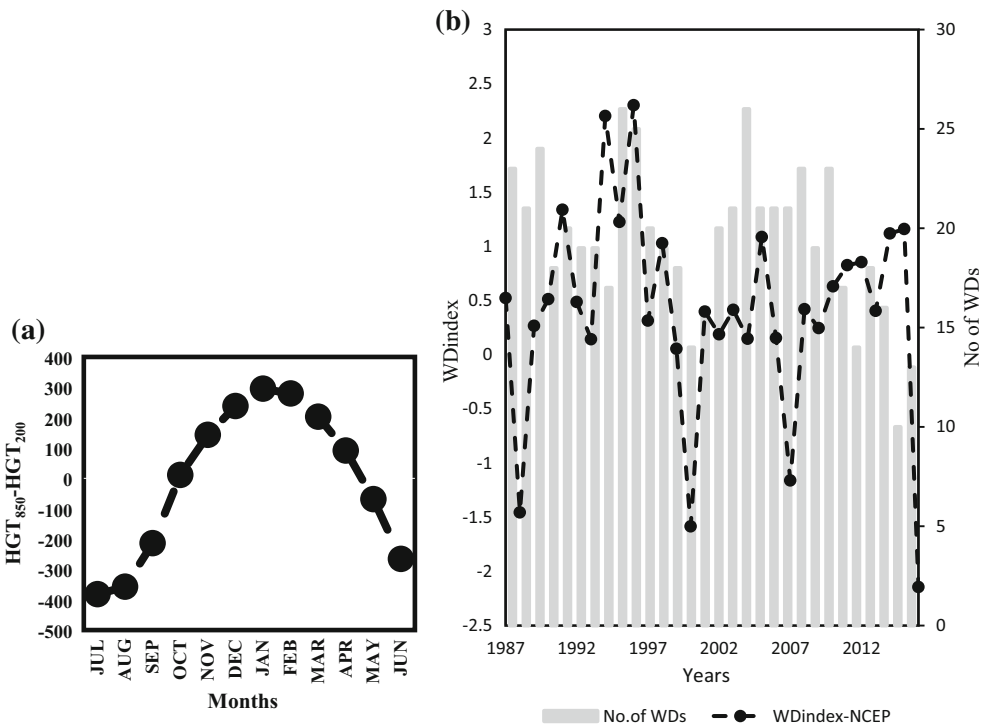

Figure 11. (**a**) Time-series of difference between geopotential height (m) anomaly at 850 and 200 hPa (850 minus 200) averaged over region 25°–40°N, 60°–80°E and (**b**) Time series of WDI and number of WDs. WDI is plotted as lines. The bar graph shows the number of WDs.

baroclinicity of basic state interplay with moist convection leads to disturbance growth. Potential vorticity anomalies influence the mean vertical shear to transfer energy from the mean baroclinicity to perturbation development (Cohen and Boos 2016).

Potential vorticity (PV) is analyzed to establish the evolution of WDs in a baroclinic background

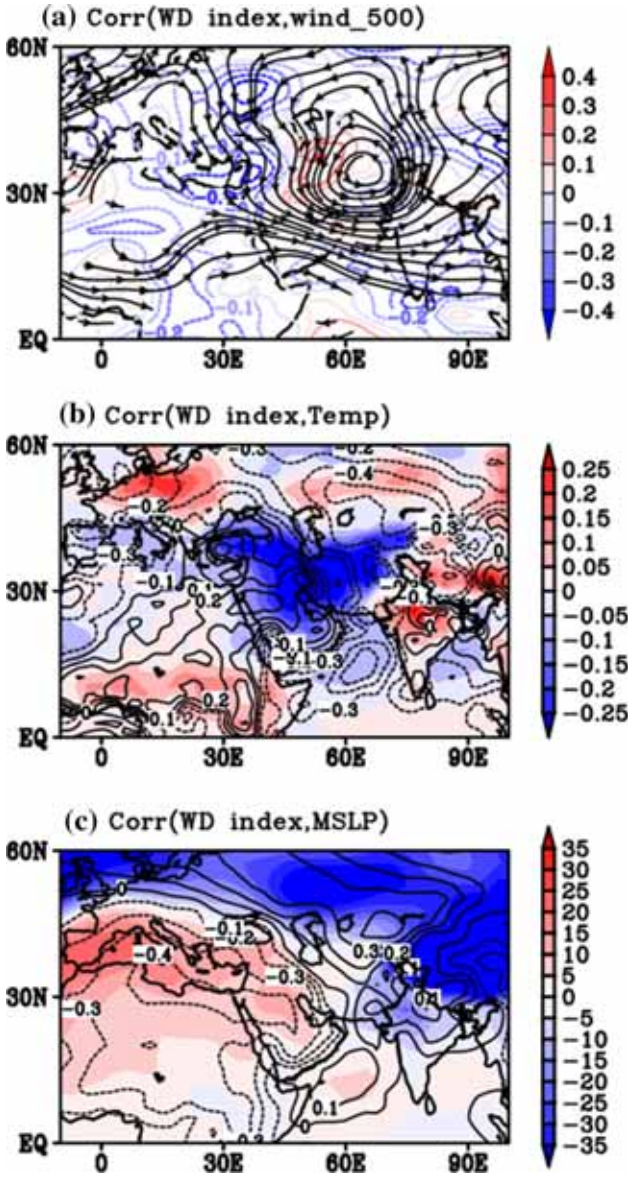

Figure 12. Spatial pattern of correlation between WDI and (**a**) 500 hPa wind (streamlines in m/s), blue contour line corresponds to negative correlation and red contour line corresponds to positive correlation, (**b**) 2m temperature (shaded in degree C), (**c**) Mean Sea Level Pressure (MSLP, shaded in meter) for WD minus DJF days averaged during 1986–2016. The positive correlation is shown in black solid contours and negative correlation is shown in broken line contours.

(figure 10) state. The structure of PV in the upper atmosphere is similar to that of baroclinic waves (Hunt *et al.* 2018b). The high value of PV is observed in cyclogenesis conditions. Low geopotential height observed over the region (figure 9a) corresponds to large PV values (figure 10a).

WDs are considered as eastward moving extratropical cyclones (Barlow *et al.* 2005). WDs are characterized by deep upper-level trough and existence of surface low (Singh and Kumar 1977). Many WD studies focus on the variability of geopotential height since it has trough in upper level. Lang and Barros (2004) noted an increase in precipitation related to WDs over CH when there is increased variability of 500 hPa geopotential height. Cannon *et al.* (2016) developed a wave tracking methodology to track WDs using 500 hPa geopotential height anomalies since WDs can be differentiated with its depression in 500 hPa geopotential height.

On account of these factors, difference between 850 and 200 hPa geopotential height anomaly (refer to Supplementary figure S1) is considered to formulate and propose WDI. The seasonal mean value of geopotential height anomaly (averaged over the area of 25°N 60°E to 40°N 80°E) at 850 and 200 hPa is calculated. Further, the value at 850 hPa is subtracted from 200 hPa. Then it is divided by standard deviation to construct standardized WDI. The index is calculated using NCEP data and further verified by using ERA-Interim reanalysis data. WDI calculated using NCEP and ERA shows almost similar values (shown in Supplementary figure S2), so for our convenience we are using NCEP WDI data in further analysis. As WDI increases temperature decreases and vice versa. WDI along with trend line is plotted against number of WDs during winter for each year and is illustrated in figure 11(b). WDI increases with number of WDs in almost all the years except in few years. This is because WDI may depend upon intensity of WDs. The correlation coefficient between WDI and number of WDs is found to be 0.1788. The poor correlation between the two may be due to the fact that not all WDs are strong enough to create large dip in upper troposphere geopotential height which leads to more precipitation over the region. Only 5% of WDs lead to heavy precipitation (Hunt *et al.* 2018b). As the intensity of WDs increases, the trough deepens in geopotential height at upper levels. Madhura *et al.* (2015) calculated WD index based on EOF analysis of daily geopotential height anomaly and standard deviation of PC1. A positive trend in WD index indicates enhanced variability in WDs and thus heavy precipitation over WH during recent periods. WDI in a way provides a comprehensive view of the vertical structure associated with the WDs. However, there are few anomalous seasons when they are not in coherence to each other and thus needs further investigation.

In order to validate the WDI, correlations between WDI with variables, viz., 500 hPa wind, 2

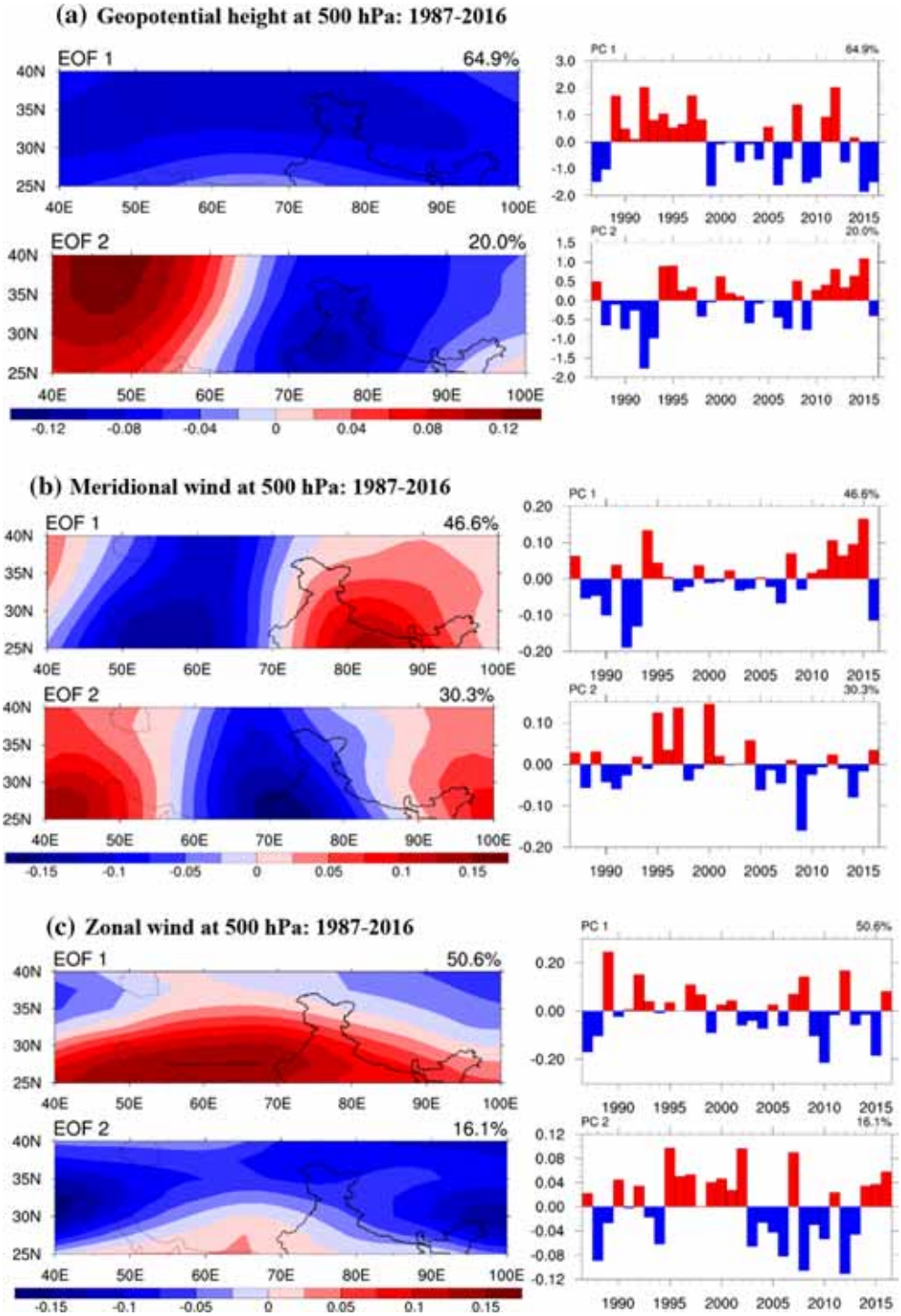

Figure 13. EOF/PC analysis of daily (**a**) geopotential height, (**b**) meridional wind and (**c**) zonal wind at 500 hPa for WD days of DJF season based on NCEP data over the domain 25–40°N,40–100°E during 1987–2016 period. The spatial pattern of the first mode is EOF1 and the spatial pattern of the second mode is EOF2. The first and second modes explain 64.9 and 20.0%, 46.6 and 30.3%, 50.6 and 16.1% of the total variance for (**a**), (**b**) and (**c**) respectively.

m air temperature and MSLP during WD minus DJF days averaged during 1986–2016 are calculated. 500 hPa wind during the WD minus DJF days averaged during 1986–2016 shows cyclonic circulation over the Himalayas and adjacent regions. 500 hPa wind is positively correlated with WDI over the Hindukush and Sulaiman range (figure 12a). That explains about the sustaining of WD over this area. A negative correlation is noted over rest of the region. This suggests a divergence of mass from the rest of the region. During the period, warmer temperature over central India and

colder temperature over regions northwest of Indian subcontinent is observed. This temperature is negatively correlated with WDI over northern India, central Asia, Arabian Sea, Indian Ocean and Bay of Bengal and positively correlated over the regions west of central Asia and central India. It is important to note that, in northern part of India warmer temperature is found which is negatively correlated with WDI (figure 12b). This suggests cold air incursion towards India during the propagation of WDs. After the passage of WDs, cold air from northern latitude moves towards India which leads to cold wave conditions (De *et al.* 2005). MSLP patterns indicate higher pressure over west of Indian subcontinent and lower pressure over India, northern latitudes and east of Indian subcontinent (figure 12c). Intense low pressure over Tibetan and central to northern India pulls the mass from Mediterranean Sea, which is an intense high-pressure region. That is why Tibetan and central to northern India is positively correlated with coefficient values 0.4–0.2. However, Mediterranean Sea, the west-south Asian region and the northeast Africa region are negatively correlated with coefficient values –0.4 to –0.2. During the passage of WDs, low-pressure area is seen over northern part of India and Pakistan. The lows are associated with ascending/converging air masses which leads to showers over the region. MSLP shows positive correlation with WDI over this region. The newly constructed WDI explains some of the variances of 500 hPa wind, 2 m air temperature and MSLP in the course of advancement of WDs over Indian region.

EOF analysis is applied to 500 hPa daily geopotential height over the domain 25–40°N, 40–100°E during the 1987–2016 period for WD days of DJF. The spatial patterns of first two EOFs (EOF1 and EOF2) and its time series known as Principal Components (PC1 and PC2) are shown in figure 13. It can be seen that EOF1 pattern shows negative all over the domain (figure 13a). More negative values are found over 30–35°N latitude. The EOF1 pattern explains 64.9% variance. PC1 shows change in amplitude of EOF1 with time. The intensity and frequency of negative amplitude are increasing in recent years. It is noted that EOF2 pattern shows negative geopotential height over WH and Pakistan and positive is seen further westward (figure 13a). Strong positive geopotential height is seen over 35°N, 45°E. EOF2 pattern shows northwest–southeast orientation. EOF2 pattern explains 20% variance. From the above analysis EOF1 can be considered as the spatial pattern of geopotential height and PC1 is the interannual variability of amplitude of EOF1 during the occurrence of WDs over the specified domain. EOF1 pattern of meridional wind explains 46.6% variance and EOF2 30.3% of total variance. While PC1 and PC2 with loading vector 0.20 to –0.20 are seen. The negative component of meridional wind delineates northerly and positive component southerly wind (figure 13b). Strong northerly wind is seen over Pakistan and southerly wind over Indian region. EOF1 pattern of zonal wind shows strong westerly jet over Pakistan and India with 50.6% variance and EOF2 explains 16.1% of total variance (figure 13c). However, PC1 shows temporal variability in range of loading vector 0.25 to –0.25. PC2 shows 0.12 to –0.12. Meridional variability of jet can be seen during the propagation of WDs. Thus, EOF1 pattern of geopotential height; zonal wind and meridional wind indicate movement of WDs over the domain.

4. Conclusions

The objective of this research is to investigate the climatology of WDs and the construction of a WDI. More than 500 WD cases from the IDWR are used to analyze the climatology of WDs. Precipitation climatology is calculated for entire winter season, during the occurrence of WDs and non-WD days and concluded that WDs produce significant amount of precipitation over WH and northern part of India during winter. WDs contribute to more than 80% of precipitation over northwest part of India and Pakistan during winter season. Vertical distribution of geopotential height and winds indicate a trough and southwesterly direction respectively during WDs which shows moisture incursion from Arabian Sea. Negative omega values at 500 hPa indicate convergence and increase in humidity which results in precipitation. A new WDI for IWM is proposed using difference of 850 and 200 hPa geopotential height and is validated using different variables such as 500 hPa wind, air temperature and MSLP. Wind at 500 hPa is positively correlated with WDI over Hindukush and Sulaiman range. Air temperature and WDI show a negative correlation over north India. Negative MSLP is positively correlated with WDI over north India. The first pattern of EOF of geopotential height, zonal wind and meridional

wind shows the propagation of WDs during winter season over the domain.

Acknowledgements

The authors acknowledge National Center for Environmental Prediction/National Centre for Atmospheric Research for providing dataset. The authors are also thankful to CPC for providing precipitation datasets. The work of Midhuna T M was supported by Junior Research Fellowship granted by Department of Science and Technology. Special thanks to Madhavi Jain for improving the English of the manuscript.

References

Ananthakrishnan R and Soman M K 1989 Statistical distribution of daily rainfall and its association with the coefficient of variation of rainfall series; *Int. J. Climatol.* **9(5)** 485–500.

Archer D R and Fowler H J 2004 Spatial and temporal variations in precipitation in the Upper Indus Basin, global teleconnections and hydrological implications; *Hydrol. Earth Syst. Sci.* **8** 47–61, https://doi.org/10.5194/hess-8-47-2004.

Ashok K, Guan Z, Saji N H and Yamagata T 2004 Individual and combined influences of ENSO and the Indian Ocean Dipole on the Indian summer monsoon; *J. Climate* **17(16)** 3141–3155, https://doi.org/10.1175/1520-0442(2004)017%3c3141:IACIOE%3e2.0.CO;2.

Barlow M, Wheeler M, Lyon B and Cullen H 2005 Modulation of daily precipitation over southwest Asia by the Madden–Julian Oscillation; *Mon. Wea. Rev.* **133(12)** 3579–3594, https://doi.org/10.1175/MWR3026.1.

Barros A P, Chiao S, Lang T J, Burbank D and Putkonen J 2006 From weather to climate – Seasonal and interannual variability of storms and implications for erosion processes in the Himalaya; In: Tectonics, Climate, and Landscape Evolution; *Geol. Soc. Am. Spec. Paper* **398** 17–38.

Benn D I and Owen L A 1998 The role of the Indian summer monsoon and the mid-latitude westerlies in Himalayan glaciation: Review and speculative discussion; *J. Geol. Soc.* **155** 353–363, https://doi.org/10.1144/gsjgs.155.2.0353.

Bookhagen B and Burbank D W 2010 Toward a complete Himalayan hydrological budget: Spatiotemporal distribution of snowmelt and rainfall and their impact on river discharge; *J. Geophys. Res.* **115(F3)**, https://doi.org/10.1029/2009JF001426.

Cannon F, Carvalho L M, Jones C and Norris J 2016 Winter westerly disturbance dynamics and precipitation in the western Himalaya and Karakoram: A wave-tracking approach; *Theor. Appl. Climatol.* **125(1–2)** 27–44, https://doi.org/10.1007/s00704-015-1489-8.

Cannon F, Carvalho L M V, Jones C and Bookhagen B 2015 Multi-annual variations in winter westerly disturbance activity affecting the Himalaya; *Clim. Dyn.* **44(1–2)** 441–455, https://doi.org/10.1007/s00382-014-2248-8.

Chen M, Shi W, Xie P, Silva V B, Kousky V E, Wayne Higgins R and Janowiak J E 2008 Assessing objective techniques for gauge-based analyses of global daily precipitation; *J. Geophys. Res.* **113**, https://doi.org/10.1029/2007JD009132.

Cohen N Y and Boos W R 2016 Perspectives on moist baroclinic instability: Implications for the growth of monsoon depressions; *J. Atmos. Sci.* **73(4)** 1767–1788, https://doi.org/10.1175/JAS-D-15-0254.1.

Dash S K, Jenamani R K, Kalsi S R and Panda S K 2007 Some evidence of climate change in twentieth-century India; *Clim. Change* **85** 299–321, https://doi.org/10.1007/s10584-007-9305-9.

De U S, Dube R K and Rao G P 2005 Extreme weather events over India in the last 100 years; *J. Ind. Geophys. Union* **9(3)** 173–187.

Dee D P, Uppala S M and Simmons A J *et al.* 2011 The ERA-Interim reanalysis: Configuration and performance of the data assimilation system; *Quart. J. Roy. Meteorol. Soc.* **137** 553–597.

Dhar O N, Kulkarni A K and Sangam R B 1984 Some aspects of winter and monsoon rainfall distribution over the Garhwal–Kumaun Himalayas – a brief appraisal; *Him. Res. Dev.* **2(2)** 10–19.

Dimri A P 2012 Wintertime land surface characteristics in climatic simulations over the western Himalayas; *J. Earth Syst. Sci.* **121(2)** 329–344, https://doi.org/10.1007/s12040-012-0166-x.

Dimri A P 2006 Surface and upper air fields during extreme winter precipitation over the western Himalayas; *Pure Appl. Geophys.* **163(8)** 1679–1698, https://doi.org/10.1007/s00024-006-0092-4.

Dimri A P 2013a Interannual variability of Indian winter monsoon over the Western Himalayas; *Global Planet. Change* **106** 39–50, https://doi.org/10.1016/j.gloplacha.2013.03.002.

Dimri A P 2013b Intraseasonal oscillation associated with the Indian winter monsoon; *J. Geophys. Res: Atmos.* **118(3)** 1189–1198, https://doi.org/10.1002/jgrd.50144.

Dimri A P and Chevuturi A 2014 Model sensitivity analysis study for western disturbances over the Himalayas; *Meteorol. Atmos. Phys.* **123(3–4)** 155–180, https://doi.org/10.1007/s00703-013-0302-4.

Dimri A P and Niyogi D 2013 Regional climate model application at subgrid scale on Indian winter monsoon over the western Himalayas; *Int. J. Climatol.* **33(9)** 2185–2205, https://doi.org/10.1002/joc.3584.

Dimri A P, Yasunari T and Kotlia B S *et al.* 2016 Indian winter monsoon: Present and past; *Earth-Sci. Rev.* **163** 297–322, https://doi.org/10.1016/j.earscirev.2016.10.008.

Dutta R K and Gupta M G 1967 Synoptic study of the formation and movement of western depression; *Indian J. Meteorol. Geophys.* **18(1)** 45.

Fairman J G, Nair U S, Christopher S A and Mölg T 2011 Land use change impacts on regional climate over Kilimanjaro; *J. Geophys. Res.* **116(D3)**, https://doi.org/10.1029/2010jd014712.

Goswami B N 1994 Dynamical predictability of seasonal monsoon rainfall: Problems and prospects; *Proc. Indian Nat. Sci. Acad. Part A* **60** 101–120.

Holton J R and Hakim G J 2012 *An introduction to dynamic meteorology*; Academic Press.

Hunt K M R, Turner A G and Shaffrey L C 2018a Extreme daily rainfall in Pakistan and North India: Scale interactions, mechanisms, and precursors; *Mon. Wea. Rev.* **146(4)** 1005–1022, https://doi.org/10.1175/MWR-D-17-0258.1.

Hunt K M R, Turner A G and Shaffrey L C 2018b The evolution, seasonality and impacts of western disturbances; *Quart. J. Roy. Meteorol. Soc.* **144(710)** 278–290, https://doi.org/10.1002/qj.3200.

Husak G J, Michaelsen J and Funk C 2007 Use of the gamma distribution to represent monthly rainfall in Africa for drought monitoring applications; *Int. J. Climatol.* **27(7)** 935–944.

Immerzeel W W, Beek L P H van and Bierkens M F P 2010 Climate change will affect the Asian Water Towers; *Science* **328(5984)** 1382–1385, https://doi.org/10.1126/science.1183188.

Jolliffe I T 2002 *Principal Component Analysis*; 2nd edn, Springer-Verlag, Berlin, Germany.

Kalnay E, Kanamitsu M and Kistler R *et al.* 1996 The NCEP/NCAR 40-year reanalysis project; *Bull. Am. Meteorol. Soc.* **77(3)** 437–471, https://doi.org/10.1175/1520-0477(1996)077%3c0437:TNYRP%3e2.0.CO;2.

Krishnamurti T N and Bhalme H N 1976 Oscillations of a monsoon system. Part I. Observational aspects; *J. Atmos. Sci.* **33(10)** 1937–1954, https://doi.org/10.1175/1520-0469(1976)033<1937:OOAMSP>2.0.CO;2.

Kutzbach J E 1967 Empirical eigenvectors of sea-level pressure, surface temperature and precipitation complexes over North America; *J. Appl. Meteorol.* **6(5)** 791–802, https://doi.org/10.1175/1520-0450(1967)006%3c0791:EEOSLP%3e2.0.CO;2.

Lang T J and Barros A P 2004 Winter storms in the Central Himalayas; *J. Meteorol. Soc. Japan* **82(3)** 829–844, https://doi.org/10.2151/jmsj.2004.829.

Madhura R K, Krishnan R and Revadekar J V *et al.* 2015 Changes in western disturbances over the Western Himalayas in a warming environment; *Clim. Dyn.* **44(3–4)** 1157–1168, http://dx.doi.org/10.1007/s00382-014-2192-7.

Mohanty U C, Madan O P, Rao P L S and Raju P V S 1998 Meteorological fields associated with western disturbances in relation to glacier basins of western Himalayas during winter season; Centre for Atmospheric Science, Indian Institute of Technology, New Delhi, Technical Report.

Mooley D A 1957 The role of western disturbances in the production of weather over India during different seasons; *Indian J. Meteor. Geophys.* **8** 253–260.

Pisharoty P R and Desai B N 1956 Western disturbances and Indian weather; *Indian J. Meteorol. Geophys.* **7** 333–338.

Puranik D M and Karekar R N 2009 Western disturbances seen with AMSU-B and infrared sensors; *J. Earth Syst. Sci.* **118(1)** 27–39, https://doi.org/10.1007/s12040-009-0003-z.

Rasmussen R, Baker B, Kochendorfer J, Meyers T, Landolt S, Fischer A P and Smith C 2012 How well are we measuring snow: The NOAA/FAA/NCAR winter precipitation test bed; *Bull. Am. Meteor. Soc.* **93(6)** 811–829.

Rangachary N and Bandyopadhyay B K 1987 An analysis of the synoptic weather pattern associated with extensive avalanching in Western Himalaya; *Int. Assoc. Hydrol. Sci. Publ.* **162** 311–316.

Rao V B and Rao S T 1971 A theoretical and synoptic study of western disturbances; *Pure Appl. Geophys.* **90(1)** 193–208, https://doi.org/10.1007/BF00875523.

Rao Y P and Srinivasan V 1969 Discussion of typical synoptic weather situation: winter western disturbances and their associated features; Indian Meteorological Department Forecast, Part III.

Rees H G and Collins D N 2006 Regional differences in response of flow in glacier-fed Himalayan rivers to climatic warming; *Hydrol. Process.* **20(10)** 2157–2169, https://doi.org/10.1002/hyp.6209.

Ridley J, Wiltshire A and Mathison C 2013 More frequent occurrence of westerly disturbances in Karakoram up to 2100; *Sci. Total Environ.* **468** S31–S35, https://doi.org/10.1016/j.scitotenv.2013.03.074.

Roy S S and Bhowmik S R 2005 Analysis of thermodynamics of the atmosphere over northwest India during the passage of a western disturbance as revealed by model analysis field; *Curr. Sci.* **88** 947–951.

Shekhar M S, Chand H and Kumar S *et al.* 2010 Climate-change studies in the western Himalaya; *Ann. Glaciol.* **51(54)** 105–112, https://doi.org/10.3189/172756410791386508.

Singh M S and Kumar S 1977 Study of western disturbances; *Indian J. Meteorol. Hydrol. Geophys.* **28(2)** 233–242.

Singh M S, Rao A and Gupta S C 1981 Development and movement of a mid tropospheric cyclone in the westerlies over India; *Mausam* **32(1)** 45–50.

Syed F S, Körnich H and Tjernström M 2012 On the fog variability over south Asia; *Clim. Dyn.* **39(12)** 2993–3005, https://doi.org/10.1007/s00382-012-1414-0.

Webster P J 1983 Mechanisms of monsoon low-frequency variability: Surface hydrological effects; *J. Atmos. Sci.* **40(9)** 2110–2124, https://doi.org/10.1175/1520-0469(1983)040%3c2110:MOMLFV%3e2.0.CO;2.

Wilks D S 1995 *Statistical Methods in Atmospheric Sciences*; Academic Press, San Diego.

Xie P, Chen M and Yang S *et al.* 2007 A gauge-based analysis of daily precipitation over east Asia; *J. Hydrometeorol.* **8(3)** 607–626, https://doi.org/10.1175/JHM583.1.

Yadav R K, Kumar K R and Rajeevan M 2012 Characteristic features of winter precipitation and its variability over northwest India; *J. Earth Syst. Sci.* **121(3)** 611–623, https://doi.org/10.1007/s12040-012-0184-8.

Yadav R K, Ramu D A and Dimri A P 2013 On the relationship between ENSO patterns and winter precipitation over north and central India; *Global Planet. Change* **107** 50–58, https://doi.org/10.1016/j.gloplacha.2013.04.006.

Yadav R K, Yoo J H, Kucharski F and Abid M A 2010 Why Is ENSO influencing northwest India winter precipitation in recent decades? *J. Climate* **23(8)** 1979–1993, https://doi.org/10.1175/2009JCLI3202.1.

Zheng X and Frederiksen C S 2007 Statistical prediction of seasonal mean southern hemisphere 500-hPa geopotential heights; *J. Climate* **20(12)** 2791–2809.

Corresponding editor: N V Chalapathi Rao